Materials Science & Engineering A 645 (2015) 323–327

Contents lists available at ScienceDirect

Materials Science & Engineering A

journal homepage: www.elsevier.com/locate/msea

Short communication

Control of interfacial intermetallic compounds in Fe–Al joining by Zn addition

J. Yang [a,b], Y.L. Li [a,*], H. Zhang [a], W. Guo [b,c], Y. Zhou [b]

[a] Key Laboratory of Robot and Welding Automation of Jiangxi Province, School of Mechanical and Electrical Engineering, Nanchang University, Nanchang, Jiangxi 330031, China
[b] Center for Advanced Materials Joining, University of Waterloo, Waterloo, Ontario, Canada N2L 3G1
[c] School of Mechanical Engineering and Automation, Beijing University of Aeronautics and Astronautics, Beijing 100191, China

ARTICLE INFO

Article history:
Received 17 June 2015
Received in revised form
9 August 2015
Accepted 10 August 2015
Available online 11 August 2015

Keywords:
Interfacial microstructure
Intermetallic compounds
Mechanical properties
Laser dissimilar joint
Al alloy and steel

ABSTRACT

By Zn addition to the fusion zone, the interfacial intermetallic compounds (IMCs) of laser Al/steel joint changed from layered Fe_2Al_5 and needle-like $FeAl_3$ to layered $Fe_2Al_{5-x}Zn_x$ and dispersed $FeZn_{10}$ with minor Al-rich amorphous phase. This resulted in an improvement in the joint strength and the change of failure mode.

1. Introduction

The evolution of interfacial intermetallic compounds (IMCs) is often encountered during the dissimilar materials processing such as welding [1], casting [2], sintering [3] and coating [4]. The mechanical properties of the welds, castings, sinters and coatings are strongly affected by the type, amount (thickness) and morphology of IMCs due to their hard and brittle nature [1–9]. It is well known that the thickness of IMCs should be controlled to less than 10 μm to obtain a sound dissimilar joint, e.g., Al/Mg [5], Al/Ti [6], Al/Cu [7], Mg/steel [8] and Al/steel [9]. Recently, Kim et al. [2] found that by controlling the morphology of FeAl-type IMCs in cast steel, the ductility of the steel was significantly enhanced, which could alleviate the harmful effects of the hard and brittle nature of the IMCs. Thus, the control of IMCs is very important in these processes.

Al and Fe are studied as a model because there are five different IMCs in the binary system, i.e., $FeAl_3$, Fe_2Al_5, $FeAl_2$, FeAl and Fe_3Al. Besides, Al alloys and steels have been widely used in industrial applications. Approaches to control Fe–Al IMCs have been extensively studied, one of which is to alter the local chemical composition by adding alloy elements, e.g., Si and Zn. The role of Si additions on the formation of Fe–Al IMCs has been established, viz., Si is able to reduce the IMCs layer thickness, and therefore improve the joint mechanical properties [10,11]. Even though Zn addition has been found to offer the possibility to improve the Al/steel joint mechanical properties, the reasons are still unclear. This is due to the unidentified interfacial IMCs in the Al/steel joint. Dharmendra et al. [12] reported that Fe_3Al was formed in the Al/steel interfacial region. Mathieu et al. [13] claimed that the interfacial IMCs were Fe_2Al_5 and $FeAl_3$. Nonetheless, most of the related literature reported that Fe–Al–Zn IMCs and an unidentified Zn-rich phase were formed in the interfacial region [14–16]. For example, Nishimoto et al. [15] found that with these kinds of interfacial phases, the laser joint exhibited a desirable joint strength even though the IMCs layer was up to 20 μm thick, which was twice the critical thickness ($\sim$10 μm) for obtaining sound Al/steel joints. Laukant et al. [16] observed that the Zn-rich phase particles were typically nano-sized.

The main purpose of this study is to clarify the role of Zn addition in the interfacial Fe–Al IMCs and the resultant joint mechanical properties by identifying interfacial phases in the Al/steel joint with Zn addition (Zn–Al filler metal) using transmission electron microscopy (TEM). Furthermore, a comparison is made between the laser joint with and without Zn (pure Al) addition in filler metal in terms of interfacial microstructure and joint strength. It was found that with the Zn addition, the type and morphology of the IMCs were altered which resulted in a significant improvement of the joint strength.

* Corresponding author.
E-mail address: liyulong1112ster@gmail.com (Y.L. Li).

http://dx.doi.org/10.1016/j.msea.2015.08.036
0921-5093/

2. Experimental

A 4 kW diode laser was used to join 1.0 mm DP 980 steel and 1.5 mm 5754 Al alloy in a lap joint configuration. The chemical composition of DP 980 steel was 0.15Cr–2.1Mn–0.35Mo (wt%); 5754 Al alloy was 2.6Mg–0.4Si–0.5Mn–0.4Fe (wt%). 1.6 mm diameter 1100 pure Al and Zn–22Al filler metals were used. A Superior No. 20 flux was used. The filler metal was placed on top of the steel sheet covered with the flux. The process parameters were 2.0 kW laser power, 0.3 m/min travel speed, and the laser beam was focused on top of the filler metal. In order to limit oxidation, argon shielding gas was provided with a flow rate of 15 l/min. The temperature of FZ during the laser joining process was measured using a thermocouple, and the cooling rate was calculated as 125.3 °C/s.

After welding, cross-sections were prepared by standard mechanical polishing techniques. The microstructure was observed scanning electron microscope (SEM) equipped with Energy-dispersive X-ray spectroscopy (EDS) analysis facility with the accuracy of 1 at% to determine the chemical composition of the interfacial phases. TEM analysis was used to confirm the phases and determine their crystallographic orientation relationships (ORs). Nanohardness of the interfacial phases was evaluated with a constant force of 4 mN. The tensile-shear testing results were the average of at least three samples. The fracture surfaces were tested by X-ray diffraction (XRD) to identify the type of interfacial IMCs.

3. Results and discussion

Fig. 1 shows the SEM image of the laser Al/steel joint with pure Al filler metal. Two distinct IMCs layers were observed at the fusion zone (FZ)/steel interface. The SEM-EDS analysis showed that layered structure point 1 contained 73Al–27Fe (at%) and the needle-like structure point 2 contained 78Al–22Fe (at%). From the XRD observation, the layered structure was identified as Fe_2Al_5 and the needle-like structure was identified as $FeAl_3$. Moreover, microcracks were evident in the Fe_2Al_5 layer. The formation of microcracks was mainly due to the inability of the hard and brittle Fe_2Al_5 layer to accommodate the thermal stress after welding [17].

Fig. 2(a) shows the SEM image of a typical cross section of the laser Al/steel joint with Zn–Al filler metal. A continuous reaction layer was observed at the FZ/steel interface having symmetrical thickness distribution around the laser beam centerline as indicated by the dashed line. The layer was about 8 µm in thickness at the toe, increased to about 35 µm at the laser beam center and decreased to about 8 µm when moving away from the center to the root (Fig. 2(b) and (c)). At zone A, the layer consisted of a dark layered structure and a light dispersed structure (Fig. 2(b)). The EDS analysis shows that the layered structure point 3 contained 64Al–30Fe–6Zn (at%), while the dispersed structure point 4 contained 9Al–6Fe–85Zn (at%). According to the Fe–Al–Zn phase diagram, the possible phases of the layered and dispersed structures were $Fe_2Al_{5-x}Zn_x$ and $FeZn_{10}$, respectively. They were confirmed by TEM as discussed later. This dispersed phase $FeZn_{10}$ was mainly nano-sized and rich in Zn, which was expected to correspond to the Zn-rich phases found but not identified in the literature [14–16]. In addition to $Fe_2Al_{5-x}Zn_x$ and $FeZn_{10}$ observed in zone A, a rod-like structure was formed at the intermediate zone B, as shown in Fig. 2(c). Since chemical composition of the rod-like phase was difficult to accurately determine by SEM-EDS, TEM analysis was performed (Fig. 3). As shown in Fig. 3(a), three distinct phases were observed. Fig. 3(b) and (c) presents the selected area diffraction patterns, which represent the incident beams $[\bar{1}12]_{Fe_2Al_{5-x}Zn_x}$ and $[0001]_{FeZn_{10}}$ zone axes which confirmed the phases identified by the SEM-EDS analysis. $Fe_2Al_{5-x}Zn_x$ was a variation of Fe_2Al_5, therefore, it shared the same crystallographic structure with Fe_2Al_5 and had similar lattice constants to Fe_2Al_5, viz., orthorhombic (lattice constants: $a=0.7656$ nm, $b=0.6415$ nm, $c=0.4218$ nm) [18]. $FeZn_{10}$ had the hexagonal crystallographic structure with the lattice constants $a=1.2787$ nm and $c=5.7222$ nm [19]. The SADPs of the rod-like structure in Fig. 3(d) showed a strong amorphous halo. According to the TEM-EDS, the rod-like structure contained 57Al–1Fe–42Zn (at%). Thus, it was determined to be an Al-rich amorphous phase. The results are consistent with those presented by Paik et al. [20] who found an Al-rich amorphous layer adjacent to $FeZn_{10}$ while investigating the dross particles formed in zinc bath after the galvannealing processes.

Tensile-shear testing showed that the joint strength of the laser joints using pure Al and Zn–Al filler metal were 730 ± 80 N and 1230 ± 60 N, respectively. The failure mode changed from interfacial failure to FZ failure (Fig. 4). The nanohardness of $FeZn_{10}$ and $Fe_2Al_{5-x}Zn_x$ were measured as 3.08 ± 0.19 GPa and 11.17 ± 0.11 GPa, respectively, which were converted to 314 ± 19 HV and 1139 ± 11 HV. While, the nanohardness of $FeAl_3$ and Fe_2Al_5 were 8.61 ± 0.23 GPa and 9.98 ± 0.56 GPa, which were converted to 879 ± 23 HV and 1018 ± 57 HV, respectively.

The Zn-rich phase reported in Refs. [14–16] was confirmed as $FeZn_{10}$ by TEM. The formation of $Fe_2Al_{5-x}Zn_x$ was apparently attributed to the diffusion and dissolution of Fe atoms towards the FZ and some Al atoms substituted by Zn atoms [21]. Nonetheless, the formation mechanism of $FeZn_{10}$ was still unclear.

It was noted that the metallurgical reactions at the FZ/steel interface in this study were similar to the interfacial reactions occurring in the hot dip galvanizing process [4]. $Fe_2Al_{5-x}Zn_x$ and $FeZn_{10}$ have been both observed at the Zn coating/steel interface in that process. There were several mechanisms for $FeZn_{10}$ formation [22], one of which was a Zn diffusion mechanism. Zn atoms from the liquid Zn bath tend to diffuse through $Fe_2Al_{5-x}Zn_x$ grain boundaries forming $FeZn_{10}$ in $Fe_2Al_{5-x}Zn_x$ or at the $Fe_2Al_{5-x}Zn_x$/steel interface. Based on this mechanism, it was possible that $FeZn_{10}$ nucleated in the $Fe_2Al_{5-x}Zn_x$ matrix and at the $Fe_2Al_{5-x}Zn_x$/steel interface. In the present study, it was evident that $FeZn_{10}$ mainly formed in the $Fe_2Al_{5-x}Zn_x$ matrix (Fig. 2). Therefore, it was considered that zinc diffusion is the formation mechanism of $FeZn_{10}$.

$Fe_2Al_{5-x}Zn_x$ was a variation of Fe_2Al_5 which included some dissolved Zn (3.5–7.5 at%) [23]. Compare Fig. 1 to Fig. 2, it was found that the microcracks were only formed in Fe_2Al_5 (1018 HV) rather than in $Fe_2Al_{5-x}Zn_x$ (1139 HV). Normally, the cracks are thought to form more readily in the harder and more brittle IMCs, which would be $Fe_2Al_{5-x}Zn_x$. However, this discrepancy is likely ascribed to the formation of $FeZn_{10}$ in the interfacial layer due to its lower hardness than other Fe–Al IMCs reported in this study. To confirm the hypothesis, the effect of $FeZn_{10}$ on interfacial

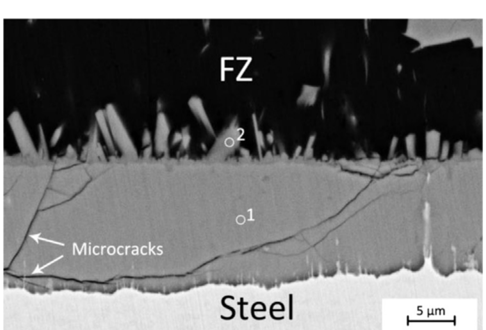

Fig. 1. SEM image of the laser Al/steel joint with pure Al filler metal.

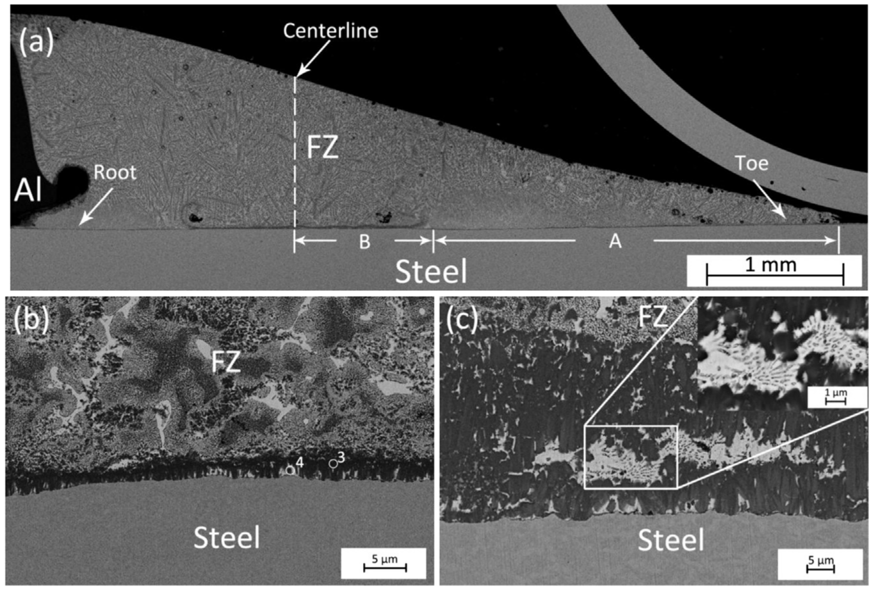

Fig. 2. SEM images of the FZ/steel interface in the laser joint with Zn–Al filler metal: (a) overall view; (b) zone A; (c) zone B, and the inset shows the higher magnification image in (c).

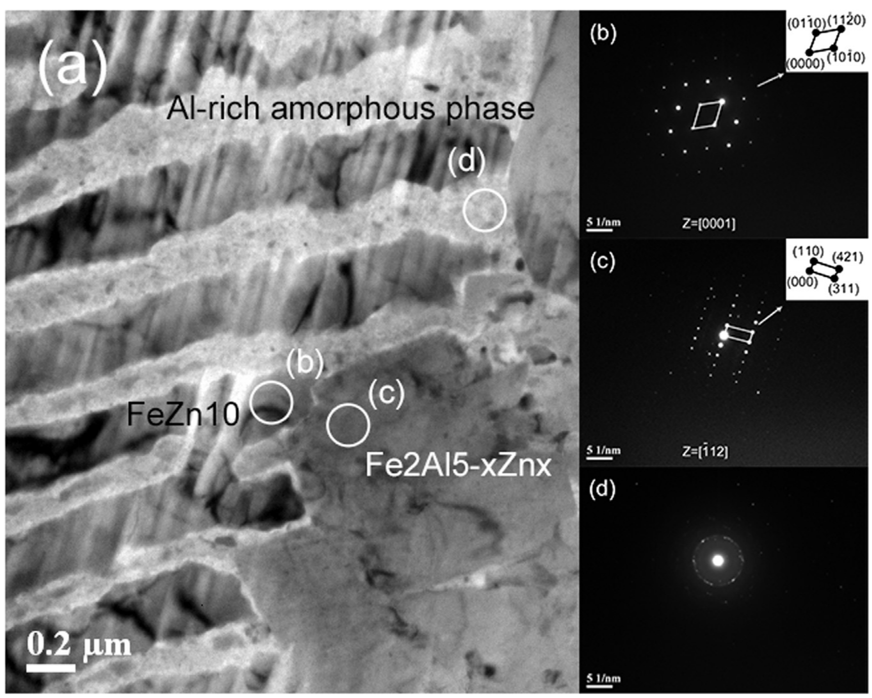

Fig. 3. TEM images of the FZ/steel interfacial layer at zone B: (a) TEM bright field image of the interfacial layer; (b), (c) and (d) selected area electron diffraction patterns (SADPs) for (b) $FeZn_{10}$, (c) $Fe_2Al_{5-x}Zn_x$ and (d) Al-rich amorphous phase indicated in (a).

microstructure was investigated in terms of crack path and interfacial strength.

A crack path in the interfacial layer was induced by indentation and is shown in Fig. 5, for which 500 g indentation force and 15 s dwell time were used. The crack in $Fe_2Al_{5-x}Zn_x$ was either deflected or arrested by the $FeZn_{10}$, rather than propagating through $FeZn_{10}$ or debonding at the interface. A similar phenomenon was observed by Schicker et al. [24], who reported that formation of such a crack path was due to the fact that the crack can easily propagate through the hard and brittle ceramic (Al_2O_3) while it could be stopped by the soft and tough metal (Fe) by plastic deformation. As a result, the composite toughness would be improved. Similarly, in this study, since $FeZn_{10}$ was less hard and brittle than $Fe_2Al_{5-x}Zn_x$, the crack could be arrested and deflected by $FeZn_{10}$. Therefore, toughness of the whole interfacial layer could be improved. In addition, $FeZn_{10}$ was mainly dispersed in $Fe_2Al_{5-x}Zn_x$, rather than forming a continuous layer. This kind of morphology, soft phase dispersed in a hard matrix, was reported in many studies, all of which mentioned its ability in promoting structure toughness [25–27]. With the combined toughening effects, the interfacial layer is enhanced and able to accommodate the thermal stress after welding, thus eliminating the formation of microcracks.

It was apparent that no debonding occurred at the $Fe_2Al_{5-x}Zn_x$/$FeZn_{10}$ interface under the indentation force, suggesting that the interface was likely to be intrinsically strong (Fig. 5). To evaluate

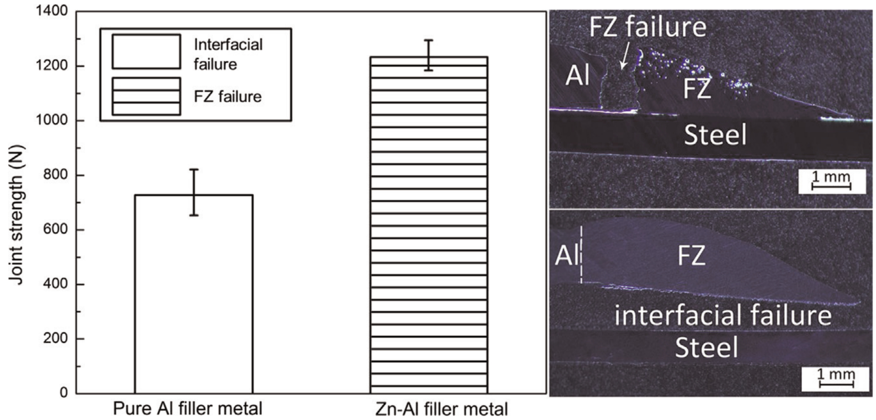

Fig. 4. Joint strength and failure modes of the laser joints with pure Al and Zn–Al filler metals.

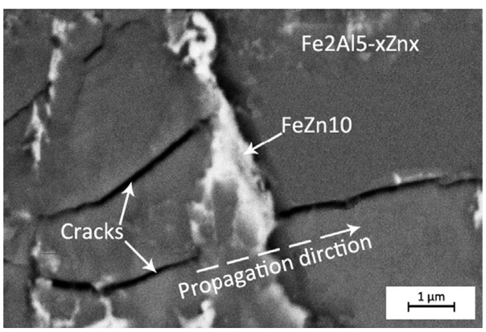

Fig. 5. Propagation path of the indentation cracks in $Fe_2Al_{5-x}Zn_x$ and $FeZn_{10}$.

the interfacial bond strength, the interfacial energy was evaluated by investigating crystallographic ORs of the $Fe_2Al_{5-x}Zn_x/FeZn_{10}$ interface. The interfacial bond strength should be directly affected by the interfacial energy which in turn depends on the degree of crystallographic registry, i.e., ORs and lattice matching, which exist between the two phases at their interface [28].

ORs of the $Fe_2Al_{5-x}Zn_x/FeZn_{10}$ interface were determined by high-resolution TEM (HR-TEM) examinations. Fig. 6 shows the HR-TEM image of the $Fe_2Al_{5-x}Zn_x/FeZn_{10}$ interface. The crystallographic orientation at the $Fe_2Al_{5-x}Zn_x/FeZn_{10}$ interface was determined to be $\{002\}_{Fe_2Al_{5-x}Zn_x}$ 29.6° from $\left\{1\bar{1}01\right\}_{FeZn_{10}}$ and the measured interplanar spacing for these planes were $\{002\}_{Fe_2Al_{5-x}Zn_x} = 2.09$ Å and $\left\{1\bar{1}01\right\}_{FeZn_{10}} = 2.13$ Å, which provided 1.9% interplanar mismatch at the interface. Liu et al. [29] pointed out that a low interplanar mismatch ($<6\%$) could provide low interfacial energy, leading to a higher interfacial bond strengths. Therefore, the HR-TEM results show an OR with sound bonding at the $Fe_2Al_xZn_{5-x}/FeZn_{10}$ interface.

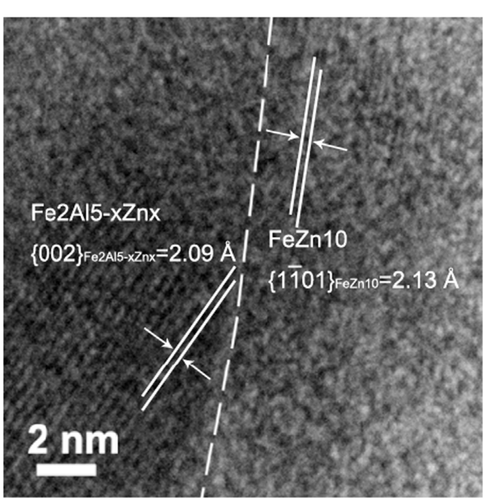

Fig. 6. HR-TEM image of the $Fe_2Al_{5-x}Zn_x/FeZn_{10}$ interface.

4. Conclusions

Interfacial IMCs significantly affect the laser Al/steel joint mechanical properties. By adding Zn to the filler metal, the interfacial IMCs change from layered Fe_2Al_5 and needle-like $FeAl_3$ to layered $Fe_2Al_{5-x}Zn_x$ and dispersed $FeZn_{10}$ with minor Al-rich amorphous phase. Consequently, the joint strength increases from 730 ± 80 N to 1230 ± 60 N and the failure mode changes from interfacial failure to FZ failure. The increase in joint strength is mainly due to the formation of $FeZn_{10}$. The improvement of joint strength by $FeZn_{10}$ is attributed to its low hardness and brittleness, dispersed distribution in $Fe_2Al_{5-x}Zn_x$ matrix and good interfacial bond strength with $Fe_2Al_{5-x}Zn_x$.

Prime novelty statement

A problem on Al/steel joint with Zn–Al filler metal raised by many researchers was that the metallurgical reaction products were not identified, which resulted in an unaccountable relationship between the microstructure and joint strength.

By using transmission electron microscopy, this paper, for the first time, identified the metallurgical reaction products and compared them to reaction products of the Al/steel joint with pure Al filler metal, thus explained that why and how the Zn addition in filler metal affected the microstructure and joint strength. This was because of the formation of $FeZn_{10}$ that had low hardness and brittleness, dispersed distribution in $Fe_2Al_{5-x}Zn_x$ matrix and good interfacial bond strength with $Fe_2Al_{5-x}Zn_x$.

Acknowledgments

Financial support of National Natural Science Foundation of China (No. 51265035), Natural Science Foundation of JiangXi Province (No. 20151BAB206042) and State Scholarship Fund of China (Grant no. 201306820002) is gratefully acknowledged. One of the authors (J. Yang) would like to thank Drs. A.M. Nasiri and P. Peng, Ph.D candidates H. Huang and D.C. Saha and MASc candidate N. Lun from the Centre for Advanced Materials Joining, University of Waterloo, for valuable discussions and proofreading. The authors thank Dr. Yuquan Ding from the Materials Science and Engineering group, University of Waterloo for assisting with nanohardness testing. The TEM research was performed at the Canadian Centre for Electron Microscopy at McMaster University, which is supported by NSERC and other government agencies.

References

[1] Y.S. Sato, S.H.C. Park, M. Michiuchi, H. Kokawa, Scr. Mater. 50 (2004) 1233–1236.
[2] S.H. Kim, H. Kim, N.J. Kim, Nature 518 (2015) 77–79.
[3] M. Łazińska, T. Durejko, S. Lipiński, W. Polkowski, T. Czujko, R.A. Varin, Mater. Sci. Eng. A 636 (2015) 407–414.
[4] A.R. Marder, Prog. Mater. Sci. 45 (2000) 191–271.
[5] V. Firouzdor, S. Kou, Metall. Mater. Trans. A 41 (2010) 2914–2935.
[6] F. Foadian, M. Soltanieh, M. Adeli, M. Etminanbakhsh, Metall. Mater. Trans. A 45 (2014) 1823–1832.
[7] H.G. Kim, S.M. Kim, J.Y. Lee, M.R. Choi, S.H. Choe, K.H. Kim, S.H. Lim, Acta Mater. 64 (2014) 356–366.
[8] A.M. Nasiri, D.C. Weckman, Y. Zhou, Weld. J. 92 (2013) 1–10.
[9] C. van der Rest, P.J. Jacques, A. Simar, Scr. Mater. 77 (2014) 25–28.
[10] J.L. Song, S.B. Lin, C.L. Yang, C.L. Fan, J. Alloy. Compd. 488 (2009) 217–222.
[11] W.J. Cheng, C.J. Wang, Intermetallics 19 (2011) 1455–1460.
[12] C. Dharmendra, K.P. Rao, J. Wilden, S. Reich, Mater. Sci. Eng. A 528 (2011) 1497–1503.
[13] A. Mathieu, R. Shabadi, A. Deschamps, M. Suery, S. Matteï, D. Grevey, E. Cicala, Opt. Laser Technol. 39 (2007) 652–661.
[14] H. Dong, W. Hu, Y. Duan, X. Wang, C. Dong, J. Mater. Process. Technol. 212 (2012) 458–464.
[15] K. Nishimoto, T. Harano, Y. Okumoto, K. Atagi, H. Fujii, S. Katayama, Weld. Int. 23 (2009) 817–823.
[16] H. Laukant, C. Wallmann, M. Müller, M. Korte, B. Stirn, H.G. Haldenwanger, U. Glatzel, Sci. Technol. Weld. Join. 10 (2005) 219–226.
[17] P. Peyre, G. Sierra, F. Deschaux-Beaume, D. Stuart, G. Fras, Mater. Sci. Eng. A 444 (2007) 327–338.
[18] L. Agudo, D. Eyidi, C.H. Schmaranzer, E. Arenholz, N. Jank, J. Bruckner, A. R. Pyzalla, J. Mater. Sci. 42 (2007) 4205–4214.
[19] S. Jazbec, P. Koželj, S. Vrtnik, Z. Jagličić, P. Popčević, J. Ivkov, J. Dolinšek, Phys. Rev. B 86 (2012) 064205.
[20] D.J. Paik, M.H. Hong, Y. Huh, J.H. Park, H.K. Chae, S.H. Park, S.Y. Choun, Metall. Mater. Trans. A 43 (2012) 1934–1943.
[21] G. Sierra, P. Peyre, F.D. Beaume, D. Stuart, G. Fras, Sci. Technol. Weld. Join. 13 (2008) 430–437.
[22] Y. Adachi, M. Arai, Mater. Sci. Eng. A 254 (1998) 305–310.
[23] G.M. Song, T. Vystavel, N. van der Pers, J.T.M. De Hosson, W.G. Sloof, Acta Mater. 60 (2012) 2973–2981.
[24] S. Schicker, T. Erny, D.E. García, R. Janssen, N. Claussen, J. Eur. Ceram. Soc. 19 (1999) 2455–2463.
[25] L. Liu, F. Liu, M. Zhu, Materials 7 (2014) 1173–1187.
[26] L.M. Liu, L.M. Zhao, R.Z. Xu, Mater. Des. 30 (2009) 4548–4551.
[27] M. Windmann, A. Röttger, W. Theisen, Surf. Coat. Technol. 226 (2013) 130–139.
[28] L. Xiao, L. Liu, S. Esmaeili, Y. Zhou, Metall. Mater. Trans. 43 (2012) 598–609.
[29] L. Liu, L. Xiao, J. Feng, L. Li, S. Esmaeili, Y. Zhou, Scr. Mater. 65 (2011) 982–985.